Stereotyped Position of Local Synaptic Targets in Neocortex

James Kozloski,* Farid Hamzei-Sichani, Rafael Yuste

The microcircuitry of the mammalian neocortex remains largely unknown. Although the neocortex could be composed of scores of precise circuits, an alternative possibility is that local connectivity is probabilistic or even random. To examine the precision and degree of determinism in the neocortical microcircuitry, we used optical probing to reconstruct microcircuits in layer 5 from mouse primary visual cortex. We stimulated "trigger" cells, isolated from a homogenous population of corticotectal pyramidal neurons, while optically detecting "follower" neurons directly driven by the triggers. Followers belonged to a few selective anatomical classes with stereotyped physiological and synaptic responses. Moreover, even the position of the followers appeared determined across animals. Our data reveal precisely organized cortical microcircuits.

The neocortex is a tissue of apparently impenetrable complexity (*1*). The cortical microcircuit, i.e., the intra- and interlaminar connections within a local neocortical region, is still largely unknown, although its characterization is essential to any theory of cortical function (*2–4*). The search for rules governing the cortical microcircuit (*1–7*) has revealed wide diversity of neurons (*7–9*), columnar (*2, 5*, *10–12*) and horizontal (*13*) connectivity, and distinct interlaminar and long-range projections (*3*, *6*, *14–17*). Connections from cortical interneurons can be precise, targeting specific postsynaptic locations (*18–20*). However, connectivity rules among excitatory cells, which constitute the vast majority of cortical neurons, remain unclear. Some studies indicate that excitatory neurons are weakly interconnected in probabilistic patterns, whereby specificity can only be found at the statistical level (*21–23*). At the same time, because the number of different classes of neocortical neurons is still unknown and could approach several hundreds (*24*), any apparent lack of target specificity might result from heterogeneous sampling. Also, physiological studies indicate remarkable circuit specificity (*5*, *25*).

We used an optical probing technique to detect postsynaptic targets of neurons in brain slices and then chose them for dual recordings (*26–28*). By imaging hundreds of neurons simultaneously while electrically stimulating a trigger cell, we optically detected which neurons ("followers") were connected to it (Fig. 1) (*29*). This approach relies on imaging action potential activity in neuronal populations loaded with calcium indicators (*30*) and enables parallel probing of connections. We chose as triggers a homogeneous population of layer 5 pyramidal cells that project to the superior colliculus (i.e., corticotectal, or CT, neurons), identified by retrograde labeling (Fig. 1, A and B) (*14–17*, *31*, *32*). CT trigger somata were located at stereotyped positions (subpial depth = 620 ± 40 μm, n = 17 cells; 17 slices; 15 mice) (*33*) and had pyramidal morphologies (*34*) and thick apical dendrites (diameter = 2.75 ± 0.75 μm at 65 μm from cell body, n = 16) with multiple collateral branches (9.5 ± 2.7 along the initial 150 μm, n = 16) and a tuft in layer 1 (Fig. 2A; Web fig. 1) (*35*). We stimulated triggers with trains of action potentials using whole-cell recording in an artificial cerebral spinal fluid (ACSF) solution that strengthened synaptic transmission (*36*) and detected simultaneous somatic calcium transients in follower cells (Fig. 1, D and E) (*37*). We then established a second whole-cell recording from followers and used dual recordings to confirm monosynaptic connections in 17 trigger-follower pairs (Fig. 1F).

We characterized the followers anatomically and physiologically. Followers belonged to three distinguishable morphological classes, confirmed with cluster analysis (Fig. 2, B and C) (*38*, *39*). Most followers were pyramidal (7/17; green in Figs. 2, B to E, and 3), followed by a second class of followers with fusiform somata (n = 6/17; red in Figs. 2, B to E, and 4, A to D) and a third class of followers (3/17; yellow in Figs. 2, B to E, and 4, E, F, and H) with large triangular somata. Finally, one follower had a small triangular soma with sparse dendrites (magenta in Figs. 2, B to E and 4, E, G, and I).

Pyramidal followers showed "dangling" basal dendrites that extended ~300 μm into layer 6 (*7*) (Fig. 3A; 3/3 cells with completely reconstructed basal dendrites). Pyramidal followers had broad spikes (half peak width = 1.21 ± 0.29 ms, n = 5) (*40*) and adaptive firing (53% ± 18 decrease in rate during 800-ms current step, n = 4; Fig. 3B). They received depressing excitatory postsynaptic currents (EPSPs) from CT neurons (5/6; Fig. 3C) (*41*). Putative contacts from trigger axons occurred onto the followers' proximal basal and apical collateral dendrites (92

Department of Biological Sciences, Columbia University, New York, NY 10027, USA.

*To whom correspondence should be addressed. E-mail: jkjames@curb.bio.columbia.edu

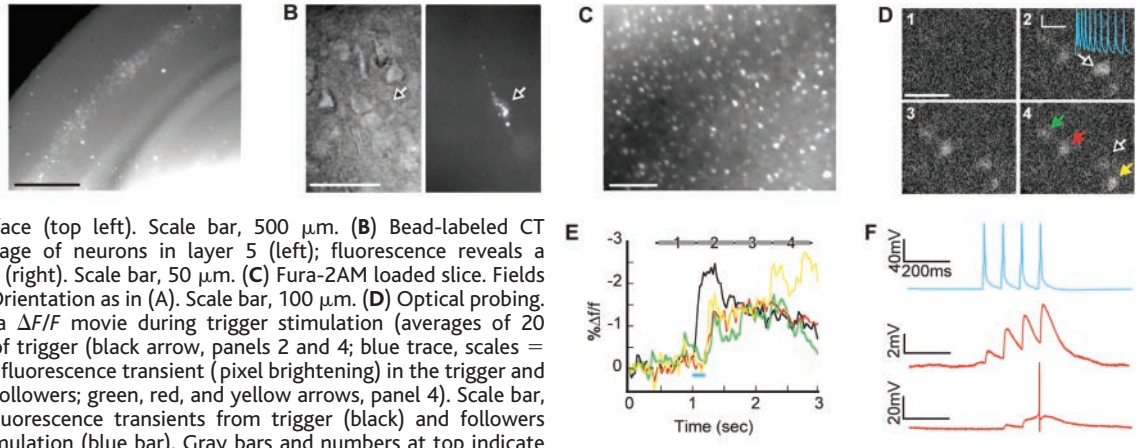

Fig. 1. Optical probing. (**A**) Retrograde labeling of CT cells. Coronal V1 slice from a mouse previously injected with rhodamine beads in the superior colliculus. Note the band of fluorescently bead-labeled cells, ~500 μm below the surface (top left). Scale bar, 500 μm. (**B**) Bead-labeled CT pyramidal neuron. DIC image of neurons in layer 5 (left); fluorescence reveals a bead-labeled pyramidal cell (right). Scale bar, 50 μm. (**C**) Fura-2AM loaded slice. Fields of layer 5 cells are loaded. Orientation as in (A). Scale bar, 100 μm. (**D**) Optical probing. Consecutive frames from a ΔF/F movie during trigger stimulation (averages of 20 frames each). Stimulation of trigger (black arrow, panels 2 and 4; blue trace, scales = 20 mV, 100 ms) results in a fluorescence transient (pixel brightening) in the trigger and in three neighboring cells (followers; green, red, and yellow arrows, panel 4). Scale bar, 50 μm. (**E**) Time-locked fluorescence transients from trigger (black) and followers (colored) during trigger stimulation (blue bar). Gray bars and numbers at top indicate frames in (D). (**F**) Dual recording confirms monosynaptic connection of trigger and follower. Whole-cell recordings from follower [red, (D) and (E)] during trigger stimulation (blue, top). The follower receives EPSPs (middle, average of 24 trials), which can cause it to spike (bottom).

μm ± 55 from somata, $n = 19$; Fig. 3A, red circles).

Fusiform followers had polarized dendrites, which were radially oriented, sparsely spiny, and beaded (Fig. 4A, 10.1 ± 3.4 spines/100 μm, 10.1 ± 4.2 beads/100 μm, $n = 6$). Axons ascended vertically (4/4) and, in one case, ramified extensively in a band 75 to 175 μm above the cell body before sending two long projections into layer 1. Electrophysiologically, these neurons showed broad spikes (1.4 ms ± 0.5, $n = 4$), weakly adaptive firing (18 ± 14% decrease, $n = 3$, Fig. 4B), and low-threshold spiking (LTS; 3/5; Fig. 4C). EPSPs from trigger cells were strongly facilitating (2/3; Fig. 4D). Putative contacts occurred primarily on secondary and tertiary dendritic branches at a characteristic distance from the somata (74 ± 36 μm, $n = 40$; Fig. 4A, yellow circles). These interneurons were classified physiologically as LTS (*42*) and resembled lower layers "ascending axon" cells (*8*) and some classes of bitufted and Martinotti cells (*19*, *23*).

Large triangular followers showed broader, more stellate dendrites than fusiform cells (Fig. 4E, major/minor axis ratio, r, of binding polygon; $r_{fusiform} = 1.6 \pm 0.28$, $r_{triangular} = 1.2 \pm 0.08$; t test $P < 0.05$), with spines and beads (13.3 ± 3.9 spines/100 μm, 12 ± 5.7 beads/μm). Axons also ascended vertically (3/3) but, unlike those of fusiform neurons, gave rise to a descending branch at a stereotyped distance from the somata (52.5 ± 2.5 μm, $n = 3$). Electrophysiologically, these neurons showed broad spikes (1.18 ± 0.23 ms, $n = 2$), adaptive firing (57 ± 31% decrease, $n = 2$, Fig. 4F, top), and, in one case, rebound spiking (Fig. 4F, bottom). These neurons received facilitating EPSPs from the triggers (2/2; Fig. 4H). Putative contacts from the trigger axons were on secondary and tertiary dendrites (125 ± 60 μm, $n = 18$). These interneurons were classified physiologically as LTS and resembled triangular cells with ascending axons described in mouse lower layers (*8*).

Finally, a small triangular follower showed polarized aspiny and moderately beaded dendrites oriented obliquely and an axon that projected medially before bifurcating into ascending and descending branches (Fig. 4E). Spikes were narrow (mean = 0.93 ms) and adapted (40% decrease) and showed a pause in all trials (Fig. 4G). This neuron was classified physiologically as fast spiking (FS) and received large, strongly depressing EPSPs (Fig. 4I).

In numerous ways, trigger-follower connections appeared specific and stereotyped from animal to animal. Pyramidal followers were different from CT cells: Their apical dendrites were thinner (1.53 ± 0.31 μm, $n = 6$; t test $P < 0.001$) and had fewer collateral branches (2.2 ± 2.1 SD, $n = 6$; t test $P \ll 0.001$). Indeed, the absence of CT neurons among the seven pyramidal followers indicates that CT neurons preferentially drove non-CT neurons to spike in our experiments. Connections from CT neurons to follower interneurons also appeared stereotyped. To characterize the background population of interneurons in mouse layer 5, we reconstructed 48 randomly sampled nonpyramidal layer 5 cells (*43*). These interneurons showed great heterogeneity in their morphologies, most of them very different from follower interneurons (see Web fig. 2A, Table 1) (*35*). Indeed, multivariate statistics ruled out that interneuron followers were randomly drawn from layer 5 interneurons [multivariate analysis of

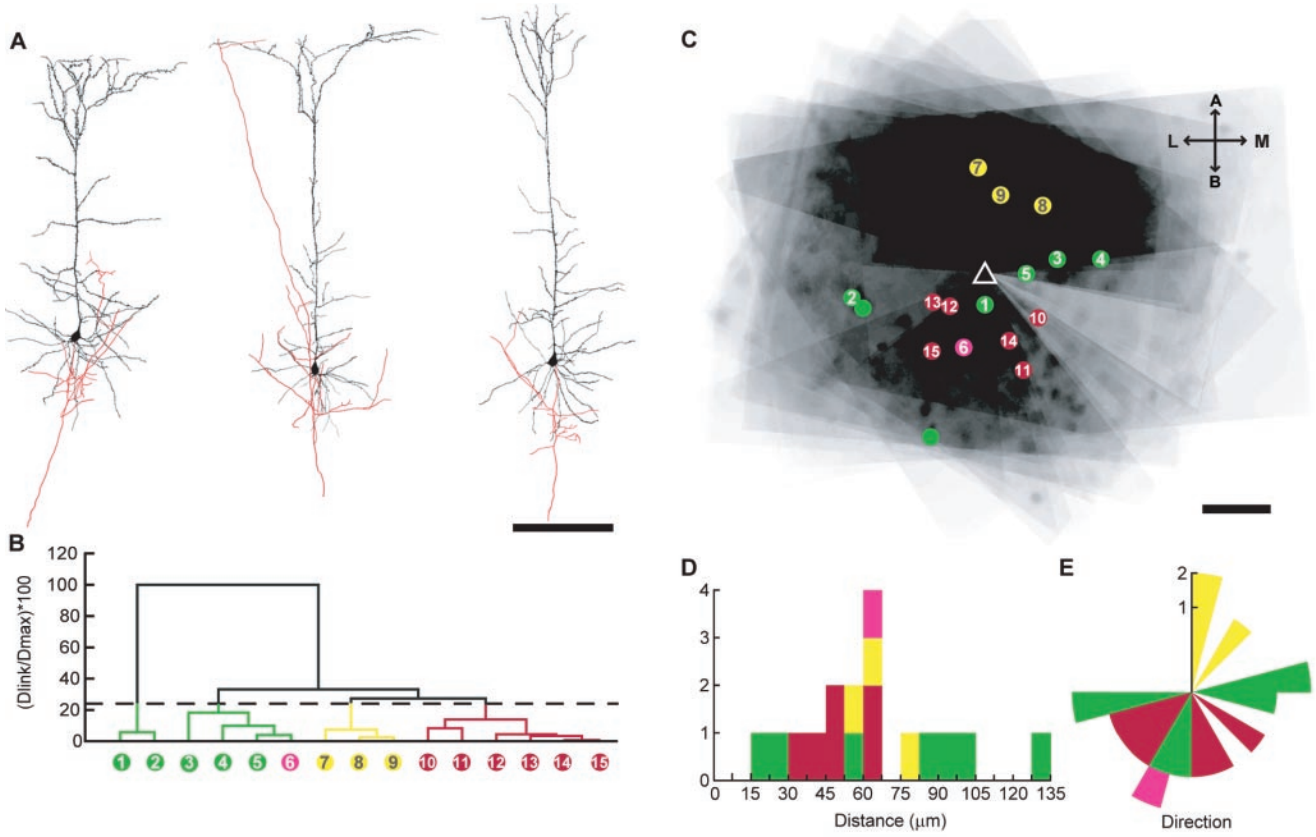

Fig. 2. Trigger cell morphology, follower classification, and positions. (**A**) Examples of three CT triggers. Dendrites are black and axons are red. Scale bar, 200 μm. See also Web fig. 1 (*35*). (**B**) Cluster analysis of followers. Four clusters were found. The first one (green) groups "dangling" pyramidal cells, the third one (yellow) groups large triangular interneurons, and the fourth one (red) groups fusiform interneurons. The second cluster (green) groups incompletely reconstructed pyramidal cells and a special interneuron (magenta) follower. (**C**) Position of followers. Follower somata [colored circles, numbered as in (B)] plotted relative to the triggers (triangle). Background represents overlay of all optical probing fluorescence images (each set to 6% opacity), with regions made optically inaccessible by trigger recording electrode deleted. Darker areas are therefore the most frequently sampled regions. A, apical; M, medial; L, lateral; B, basal: orientation to triggers in all figures. Scale bar, 50 μm. (**D**) Distributions of distance and (**E**) direction of followers' somatic positions relative to those of the triggers. Colors as in (B).

variance (MANOVA); Wilks' lambda = 0.8; $P < 0.05$] (*44*). Furthermore, cluster analysis independently showed that interneuron followers represent only a few of the different types of layer 5 interneurons (see Web fig. 2B) (*35*).

In addition, we noticed that even the somatic positions of the followers were predictable from animal to animal (Fig. 2C). Although triggers were located at a restricted subpial depth, the locations of the three major classes of followers relative to their triggers appeared precisely determined (Fig. 2, D and E), with variances much smaller than that of the depths of the triggers. Fusiform followers were always located below and at a distance of ~50 μm (51.2 ± 12.2 μm, $n = 6$) from triggers, forming a semicircle (Fig. 2, C to E). Meanwhile, triangular followers were located ~65 μm above triggers (66.2 ± 9.5 μm, $n = 3$). At the same time, pyramidal followers were located in a narrow horizontal band that included triggers (6/7 followers). We tested the positional stereotypy of followers using four independent statistical approaches: (i) The positions of follower interneurons fell along preferred directions from the triggers (Rayleigh's vector average, $R_{\text{fusiform}} = 0.74$, $P < 0.05$; $R_{\text{triangular}} = 0.96$, $P < 0.05$), (ii) these directions were not skewed by the positions of all optically probed cells (test of mean directions; $P < 0.05$), (iii) the observed fusiform cells' position below their triggers was significantly different from the expected one, based on the positions of all probed somata ($\chi^2 = 7.4$, $P < 0.01$), and (iv) the stereotyped regions occupied by follower interneurons' dendrites were poorly correlated to the regions covered by trigger axons (pairwise linear regression of axonal and dendritic probability density contour plots; $R_{\text{fusiform}} = 0.29$; $R_{\text{triangular}} = 0.03$) (*45*, *46*).

Using a method to optically reveal connections, we encountered stereotyped local synaptic circuits in neocortex. Although our results could be influenced by many experimental factors, they can nevertheless reveal stereotyped circuits only if they indeed exist. Neurons activated by CT cells fell into a few anatomically and physiologically homogeneous types, which represented a small subset of those present in layer 5 (see Web fig. 2) (*4*, *8*, *19*, *35*, *47*, *48*). Moreover, even the position of these targeted neurons appeared determined in different animals and was remarkably precise, indicating robust developmental control of circuit formation.

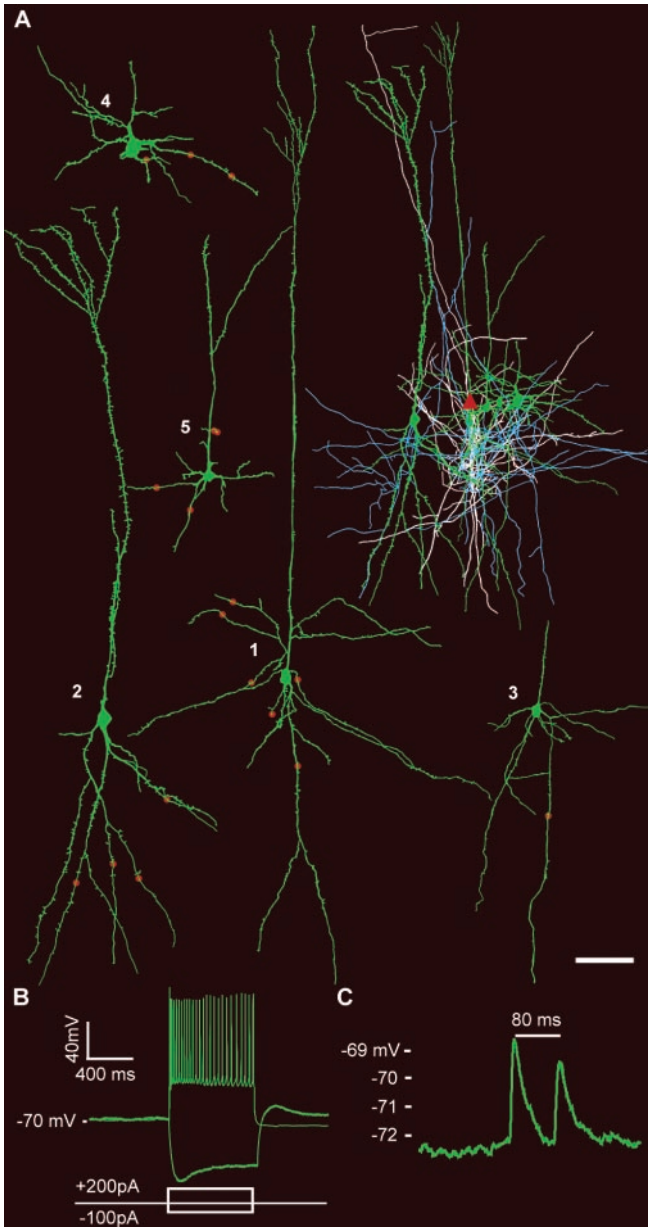

Fig. 3. Pyramidal followers. (**A**) Anatomical reconstructions. Each pyramidal follower is depicted twice: (i) top right, all followers from different slices are overlaid relative to the trigger cells (red triangle; scale bar, 100 μm), with follower axons shown in blue and trigger axons in white, and (ii) surrounding, follower cell bodies and dendrites, positioned so as not to overlap (scale bar, 70 μm). Cells are numbered as in Fig. 2. Note dangling basal dendrites and thin apical dendrites. Putative axonal contacts are indicated with red circles. (**B**) Regular-spiking firing of pyramidal follower. (**C**) Paired-pulse depression of CT to pyramidal follower EPSPs.

References and Notes

1. S. Ramón y Cajal, *Recuerdos de mi vida: Historia de mi labor científica* (Alianza Editorial, Madrid, 1923; reedited 1981).
2. V. B. Mountcastle, *Perceptual Neuroscience: The Cerebral Cortex* (Harvard Univ. Press, Cambridge, MA, 1998).
3. R. J. Douglas, K. A. C. Martin, in *The Synaptic Organization of the Brain*, G. M. Shepherd, Ed. (Oxford Univ. Press, Oxford, 1998), chap. 12.
4. P. Somogyi, G. Tamas, R. Lujan, E. H. Buhl, *Brain Res. Brain Res. Rev.* **26**, 113 (1998).
5. D. H. Hubel, T. N. Wiesel, *Proc. R. Soc. London Ser. B Biol. Sci.* **198**, 1 (1977).
6. C. D. Gilbert, *Annu. Rev. Neurosci.* **6**, 217 (1983).
7. S. Ramón y Cajal, *La Textura del Sistema Nerviosa del Hombre y los Vertebrados* (Moya, Madrid, 1904).
8. R. Lorente de Nó, *Trab. Lab. Invest. Biol. Madrid* **20**, 41 (1922).
9. A. Peters, E. G. Jones, *Cerebral Cortex* (Plenum, New York, 1984).
10. R. Lorente de Nó, in *Physiology of the Nervous System*, J. F. Fulton, Ed. (Oxford Univ. Press, New York, 1949), pp. 274–301.
11. V. B. Mountcastle, in *The Mindful Brain*, G. M. Edelman, V. B. Mountcastle, Eds. (MIT Press, Cambridge, MA, 1978), chap. 1.
12. J. Szentagothai, *Proc. R. Soc. London Ser. B Biol. Sci.* **201**, 219 (1978).
13. C. D. Gilbert, T. N. Wiesel, *J. Neurosci.* **3**, 1116 (1983).
14. B. R. Schofield, L. E. Hallman, C. S. Lin, *J. Comp. Neurol.* **261**, 85 (1987).
15. M. Hubener, J. Bolz, *Neurosci. Lett.* **94**, 76 (1988).
16. E. M. Kasper, J. Lubke, A. U. Larkman, C. Blakemore, *J. Comp. Neurol.* **339**, 495 (1994).
17. A. Rumberger, M. Schmidt, H. Lohmann, K. P. Hoffmann, *Exp. Brain Res.* **119**, 375 (1998).
18. E. H. Buhl, K. Halasy, P. Somogyi, *Nature* **368**, 823 (1994).
19. A. Gupta, Y. Wang, H. Markram, *Science* **287**, 273 (2000).
20. P. Somogyi, T. F. Freund, A. Cowey, *Neuroscience* **7**, 2577 (1982).
21. E. L. White, *Cortical Circuits: Synaptic Organization of the Cerebral Cortex, Structure, Function, and Theory* (Birkauser, Boston, MA, 1989).
22. M. Abeles, *Corticonics: Neural Circuits of the Cerebral Cortex* (Cambridge Univ. Press, Cambridge, 1991).
23. V. Braitenberg, A. Schütz, *Cortex: Statistics and Geometry of the Neuronal Connectivity* (Springer, Berlin, ed. 2, 1998).
24. B. Solnick, T. L. Davis, P. Sterling, *Proc. Natl. Acad. Sci. U.S.A.* **81**, 3898 (1984).
25. R. C. Reid, J. M. Alonso, *Nature* **378**, 281 (1995).
26. Z. A. Peterlin, J. Kozloski, B. Q. Mao, A. Tsiola, R. Yuste, *Proc. Natl. Acad. Sci. U.S.A.* **97**, 3619 (2000).
27. PND 14-16 C57 Bl/6 mice were anesthetized and perfused with cold (4°C) ACSF containing 27.06

mM sodium bicarbonate, 1.5 mM sodium phosphate monobasic, 222.15 mM sucrose, 2.58 mM KCl, 3 mM $MgSO_4$, and 1 mM $CaCl_2$. Three hundred fifty micrometer slices were cut on a vibratome (Leica). Slices were transferred to warm (37°C), oxygenated ACSF (3 $MgSO_4$ and 1 $CaCl_2$) and allowed to equilibrate to room temperature.

28. We used a double incubation loading protocol: (i) an initial application of 10 μl of 1 mM fura-2 AM (Molecular Probes; in 100 % DMSO) for 2 min and (ii) a second incubation in 1.5 ml of 30 μM fura-2 AM in ACSF for 60 min.
29. We imaged somata of fura-labeled cells in layer 5 with a ×40/0.8 NA objective (Olympus), a 385-nm excitation filter (Chroma), and a SIT Camera (Dage)

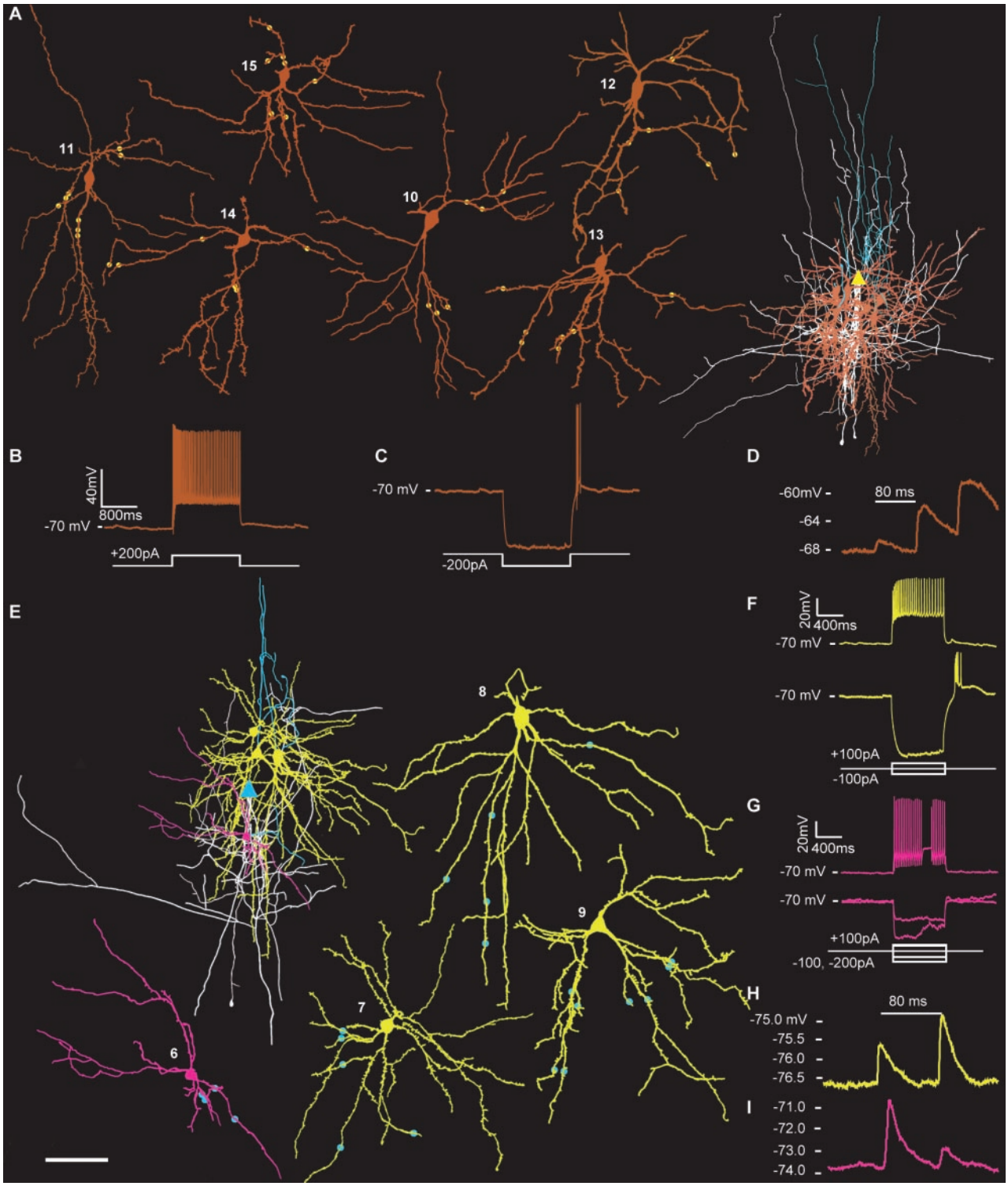

Fig. 4. Fusiform followers: (**A**) Anatomical reconstructions. Fusiform followers and scale bar depicted as in Fig. 3. Note polarized dendrites and putative axonal contacts in yellow. (**B**) Adaptive firing of fusiform follower to depolarizing current step. (**C**) LTS evoked by hyperpolarizing pulse. (**D**) Facilitation of CT to fusiform EPSPs. Triangular followers: (**E**) Anatomical reconstructions. Triangular followers and scale bar as in Fig. 3. Putative axonal contacts are indicated by blue circles. (**F**) Intrinsic firing of triangular followers. Top: adaptive spiking. Bottom: LTS. (**G**) Intrinsic firing of small triangular follower. Top: pausing spike train. Bottom: lack of LTS. (**H**) Paired-pulse facilitation of CT to large triangular follower EPSPs. (**I**) Paired-pulse depression of CT to small triangular follower EPSPs.

connected to a frame grabbing board (Scion LG3) in a Macintosh computer. Frames were acquired at ~30 ms/frame and analyzed with NIH-Image.
30. D. Smetters, A. Majewska, R. Yuste, *Methods* **18**, 215 (1999).
31. L. C. Katz, A. Burkhalter, W. J. Dreyer, *Nature* **310**, 498 (1984).
32. Injections of fluorescent latex microspheres (Lumafluor) were made into the superior colliculus, 2 to 4 days before the experiment. Injection coordinates were tailored to the age.
33. We report SD in all measurements.
34. Every trigger-follower pair was recorded with biocytin-filled electrodes to recover morphologies following standard procedures (*26*). Neurons were reconstructed with a ×40/1.00 NA objective, and contacts were identified with a ×100/1.3 NA objective.
35. Supplementary information is available at www.sciencemag.org/cgi/content/full/293/5531/868/DC1.
36. To maximize followers' detection, we used ACSF containing 126 mM NaCl, 3 mM KCl, 26 mM $NaHCO_3$, 1 mM NaH_2PO_4, 2 mM CaCl2, 1 to 2 mM $MgSO_4$, 10 mM dextrose, 5 μM nicotine, 0.5 μM 4-aminopyridine (4AP), and 0.5 μM bicuculline. Followers can also be detected with normal or Mg-free ACSF (*26*). Experiments were done at 27°C. One to four followers were observed per trigger neuron, and followers chosen for dual recordings were reliably detected optically in 70 ± 38% of subsequent trials. Whole-cell recordings were performed with 6 to 9 megaohm pipettes, filled with 130 mM K-methylsulfonate, 11 mM biocytin, 10 mM KCl, 10 mM Hepes, 5 mM NaCl, 2.5 mM Mg–adenosine triphosphate, 0.3 mM Na–guanosine triphosphate, and 0 to 0.05 mM fura-2 pentapotassium salt (Molecular Probes). Dual recordings were made with an Axopatch 200B (Axon Instruments) and a BVC-700 (Dagan Instruments) amplifier and digitized with an A/D board (Instrutec) with Igor (Wavemetrics). For optical probing, a stereotyped spike train was used (10 pulses adapting over 200 ms, blue in Fig. 1D).
37. For each pixel, we defined the fluorescence change over time as $\Delta F/F = (F_1 - F_0)/F_0$, expressed in %, where F_1 is fluorescence at any time point and F_0 is fluorescence at the beginning of each trial. We tailored the imaging and analysis protocols to the kinetics of somatic calcium signals. To detect followers online, we computed a $\Delta F/F$ movie and adjusted the look-up table so that pixels recording calcium increases appeared light over a black background (Fig. 1D).
38. G. A. Marcoulides, S. L. Hershberger, *Multivariate Statistical Methods* (Lawrence Erlbaum Associates, Mahwah, NJ, 1997).
39. For each reconstructed neuron, we measured 18 morphological variables describing soma size and shape, dendrite number and total length, circular distribution of dendrites (vector averages), size and shape of the dendritic arborization (tile), distribution of dendrites along the radial axis, and depth of axonal ramification (Web table 1) (*35*). The positional data were not included in the cluster analysis. From these variables, we extracted the five principal components for follower clustering (Fig. 2B; eigenvalues > 1.0; Statistica) that accounted for most of the observed variance (89%); only the 11 standardized variables that made up the significant principal coordinates (absolute value > 0.7) were used. For large interneuron clustering (Web fig. 2B) (*35*), all variables were included and weighted as described below (*44*). Cluster analyses were performed with Ward's method (Statistica) and squared Euclidian distances.
40. Spike half-widths were averaged across at least 10 spikes in each cell, and means were averaged across cells in a class.
41. To measure facilitation and depression, we averaged responses to pairs of spikes (80-ms interval) over at least 10 trials and computed the mean changes in averaged EPSP peak amplitudes across cells in a class. In some instances, three to four spikes were presented at 80-ms intervals.
42. Responses in all interneurons were blindly classified as LTS or FS on the basis of standard criteria (M. Beierlein, personal communication).
43. For random sampling of interneurons, layer 5 neurons without apical dendrites were patched. Physiological responses to 800-ms current steps were examined to further confirm the nonpyramidal identity of recorded neurons.
44. To compare follower interneurons (n = 10) with the random sample (n = 48), we measured 19 variables from all cells. Our null hypothesis, that trigger axons contact interneurons randomly, was tested by comparing the original distribution of follower types with the density distribution of each randomly selected interneuron type in the neuropil. To achieve this, we weighted each randomly selected neuron on the basis of the length of its dendrites projected onto a plane, normalized to the cell with the longest dendrites. Weights were assigned on an integer scale from 1 to 10 (10 being the longest), and the MANOVA was significant both with and without a single outlier whose dendritic lengths exceeded the mean by 4 SD (upper left cell in Web fig. 2A) (*35*); all remaining weighted neurons' dendritic lengths were within 2 SD of the mean.
45. A. Swan, M. Sandilands, P. McCabe, *Introduction to Geological Data Analysis* (Blackwell Sciences, Oxford, 1995).
46. To correlate the axonal and dendritic arborizations, we constructed pairs of normalized probability density contour plots, using a 40-μm region surrounding each process, and calculated the linear correlation between plots (Matlab).
47. A. Fairen, J. DeFelipe, J. Regidor, in *Cerebral Cortex*, vol. I, A. Peters, E. G. Jones, Eds. (Plenum, New York, 1984), pp. 201–255.
48. J. S. Lund, *Annu. Rev. Neurosci.* **11**, 253 (1988).
49. We thank S. Giboni, Z. Peterlin, G. Tamas, and A. Tsiola for help and members of the laboratory for comments. This work was funded by the National Eye Institute, the National Institute of Mental Health, and the National Institute of Neurological Disorders and Stroke.

20 March 2001; accepted 12 June 2001

Sorting of Striatal and Cortical Interneurons Regulated by Semaphorin-Neuropilin Interactions

Oscar Marín,[1] Avraham Yaron,[2] Anil Bagri,[2] Marc Tessier-Lavigne,[2] John L. R. Rubenstein[1]*

Most striatal and cortical interneurons arise from the basal telencephalon, later segregating to their respective targets. Here, we show that migrating cortical interneurons avoid entering the striatum because of a chemorepulsive signal composed at least in part of semaphorin 3A and semaphorin 3F. Migrating interneurons expressing neuropilins, receptors for semaphorins, are directed to the cortex; those lacking them go to the striatum. Loss of neuropilin function increases the number of interneurons that migrate into the striatum. These observations reveal a mechanism by which neuropilins mediate sorting of distinct neuronal populations into different brain structures, and provide evidence that, in addition to guiding axons, these receptors also control neuronal migration in the central nervous system.

Most striatal and cortical interneurons derive from a distant region in the basal telencephalon, the medial ganglionic eminence (MGE) (*1–3*). During development, interneurons migrate tangentially along stereotypical pathways to reach the striatum and the cortex, but the mechanisms that regulate their segregation into these two telencephalic subdivisions are not known.

To study the tangential migration of telencephalic interneurons, we used slice cultures (*4*) and transplanted portions of the MGE from green fluorescent protein (GFP)–expressing transgenic mice (*5*) into host slices obtained from wild-type littermate embryos (Fig. 1). In agreement with previous reports (*1–4*), this assay consistently labeled a large number of migrating neurons whose transmission is mediated by γ-aminobutyric acid (GABA) (*6*). GFP-expressing cells followed two major routes in the basal telencephalon. Early migrations occurred superficial to the striatum [embryonic day 12 (E12); Fig. 1, A to D] (*7*), whereas later migrations (E13.5 and older) occurred primarily deep to the striatum (Fig. 1, E to H). Cells migrating toward the cortex seemed to avoid the striatum (Fig. 1, A to H), raising the possibility that cortical interneurons might be instructed to avoid the striatum to promote their migration into cortical territories. To test this hypothesis, we transplanted striatal tissue into the cortex (Fig. 1I). GFP-expressing cells migrating from the MGE avoided the ectopic striatum (Fig. 1, J and K), but migrated normally when a piece of piriform cortex was transplanted into the same location (Fig. 1, K to M).

[1]Department of Psychiatry, Nina Ireland Laboratory of Developmental Neurobiology, Langley Porter Psychiatric Institute, [2]Department of Anatomy, Howard Hughes Medical Institute (HHMI), and Department of Biochemistry and Biophysics, University of California, San Francisco, CA 94143, USA.

*To whom correspondence should be addressed. E-mail: jlrr@cgl.ucsf.edu